MANUFACTURING TRIALS OF A RIBBED TUBE FOR THE SPIKED CONCEPT AIR PREHEATER

Jaap Hoffmann and Ben Brand

Dept. of Mechanical and Mechatronic Engineering, Stellenbosch University, Private Bag X1, Matieland, 7602, South Africa.

Phone: + 27 21 808 3554; E-mail: hoffmaj@sun.ac.za

Abstract

The tall internal fins required by the original design of the spiked concept receiver are expensive to manufacture. Various cheaper alternative configurations, concentrating on ease of manufacture, were considered. Spike performance was evaluated using CFD. Enclosing corrugated fins in a sleeve offers the best solution in terms of heat transfer and pressure drop, outperforming the original design on both counts. Decreasing the number of fins gave the highest increase heat transfer, at the cost of an increase in pressure drop. Heat transfer enhancement inside the dome reduced the metal temperatures.

Keywords: Spiked concept receiver; manufacturing process; CFD simulation.

1. Introduction

Solar thermal power with thermal energy storage is virtually available on demand. As a result, it offers value that cheaper forms of renewable energy, such as photovoltaics (PV) and wind cannot match at present. However, being more expensive than wind and PV, lags behind in terms of energy market share. Despite the steep drop in cost recently [1], large scale roll-out remain slow. This hampers further cost reduction due to learning and mass production. Installed capacity tends to favour parabolic trough plant with thermal oil as heat transfer fluid, and two-tank molten salt thermal energy storage. Central receiver plant using molten salt as heat transfer fluid and thermal energy storage benefits from higher thermal efficiencies due to the higher operating temperatures that can be reached. Thermal energy storage at direct steam plants is constrained. All these plants discussed so far rely on a steam driven Rankine cycle for the power block. One advantage of steam turbines is their vast operating history in fossil fuel plants all over the world.

A Brayton cycle offers even higher thermal efficiencies, provided that the required temperature and pressures can be reached. Furthermore, the high turbine outlet temperature from a gas turbine makes it amenable to cogeneration. This has prompted Kröger [2] to propose the SUNSPOT cycle depicted in figure 1. The SUNSPOT cycle comprise of a solarized gas turbine, and an asynchronous dry-cooled steam turbine, coupled by a rock bed thermal energy storage system. The gas turbine would run mainly during the day, whilst the steam turbine will operate mainly at night. Lower air temperatures at night would also benefit the air cooled condenser. If required, the inlet temperature to the gas turbine may be boosted by co-firing of a fossil fuel.

One draw-back that has hampered the development of solarized gas turbines at utility scale is a cheap and robust receiver capable of delivering air temperatures up to a 1 000 °C. The highest temperatures were achieved by the Weissman Institute's DIAPPR receiver [3], and the German AeroSpace Centre's REFOS receiver [4]. Both receivers use a quartz window to contain the high pressure gas, whilst allowing solar radiation in. A somewhat similar receiver was developed by the Swiss Federal Institute of Technology [5]. It remains doubtful if these can be up-scaled to utility size [6]. Comprehensive reviews of more recent high temperature receiver developments are offered by Ávila-Marín [7] and Ho and Iverson [8].

Lubkoll et all [9] developed the spiked concept receiver shown in figure 2. The receiver comprise of spikes pointing radially outwards on a spherical dome. Spikes are annular in structure, with cold pressurized air flowing through the inner pipe. A jet of cold air impinges on the spherical end cap where the stagnation flow causes high local heat transfer coefficients. This is also where the highest incident radiation for the collector field is expected. Warm air returns via the finned annular space, where it picks ups more heat through the sides of the tube to achieve a volumetric effect. The fins serve to enhance the heat transfer surface area in the annulus. Lubkoll predicts that an air outlet temperature of 800 °C, and a receiver efficiency of about 70 %, can be reached. His estimates are based on a 50 MW_t receiver.

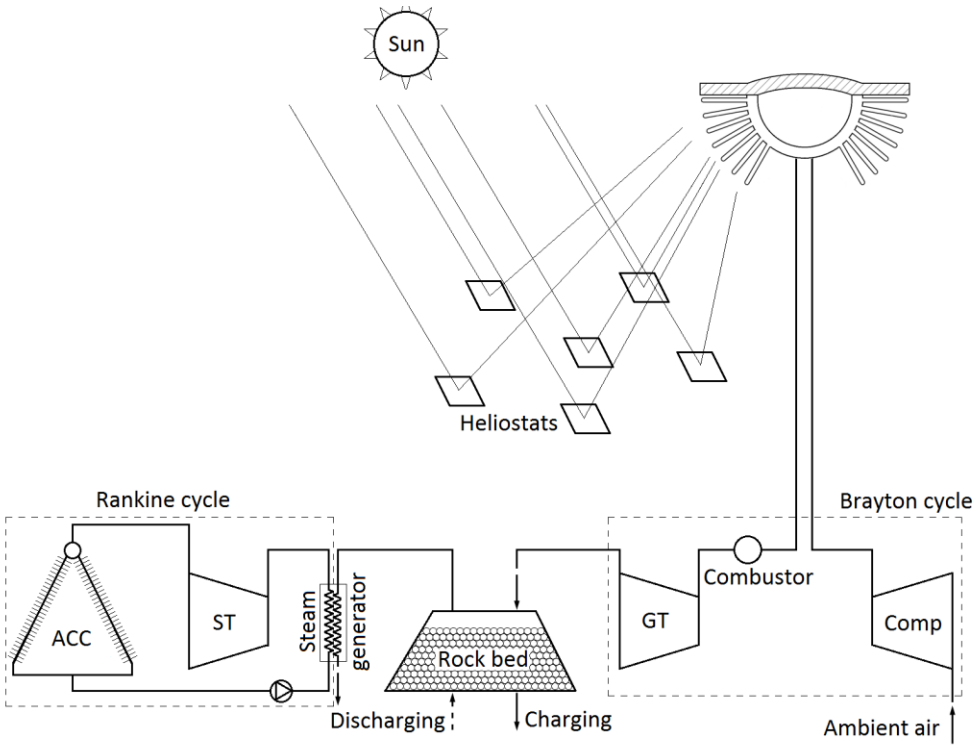

Figure 1. Schematic for the SUNSPOT cycle

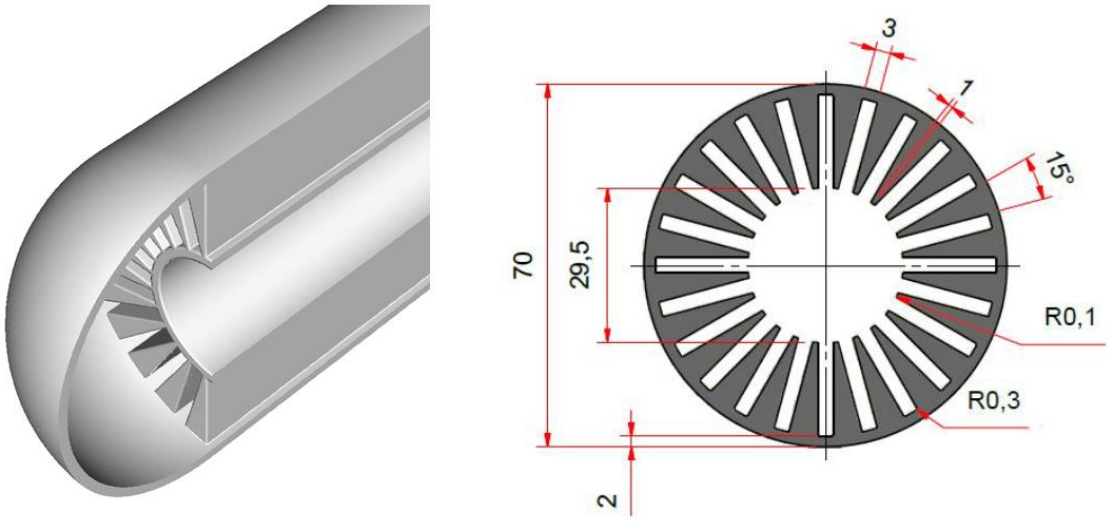

Figure 2. Original spiked concept receiver

Test specimens for Lubkoll's work were prepared by wire cutting. However, the high machining cost, and limited size of the specimen would drive up the receiver, and hence overall plant cost way beyond what would be tolerable on commercial plant. This paper describes a derivative of the spiked receiver that should be cheap and easy to manufacture. Initial thermal and structural analyses point towards successful implementation.

Degroote [10] and McDonald et al [11] both proposed similar concepts for longitudinal fins made from a single sheet of

corrugated metal, to be inserted into the annular space between two tubes. The fin tips are clad with a lower temperature metal to facilitate braising of fins to the tubes. Degroote suggested u-shaped fins, whilst McDonald et al preferred v-shaped fins, with holes punched in the fin membrane to enhance heat transfer in the annular space. Their emphasis is on heat transfer from the inner fluid stream to the outer fluid stream.

2. Concept description

Here, we propose a concept whereby a sheet of metal is bent into 24 fins, and then rolled into a circle to form the internally finned tube, as shown in figure 3. Unconstrained, the corrugations tend to open under pressure and radial displacements of up to 20 mm were predicted using a commercial finite element analysis code. Equally spaced retaining rings on the outside maintain structural integrity of the corrugated section under pressure. A smooth tube is inserted through the middle to allow cold compressed air to enter. A spherical end cap forces the air to turn through 180° degrees and return through the corrugated section. A sealing disk between the end cap and corrugated section separates the compressed from the ambient air.

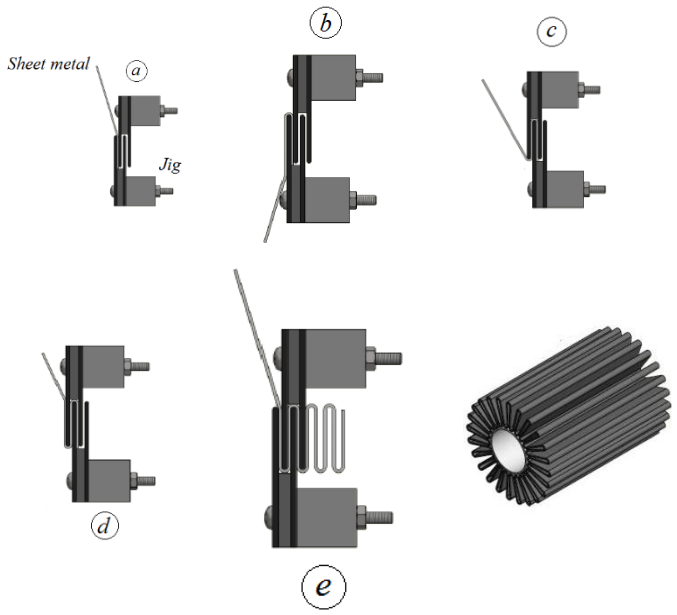

Figure 3. Jig, bending procedure and final product.

Solar radiation can penetrate into the space between fins, enlarging the heat transfer surface by more than 300 %. Furthermore, heat is conducted across the material thickness only, not down fins, reducing the conduction resistance between the outside and inside of the tube. Although the proposed concept uses 30 % less material, peak stresses under pressure are almost doubled. The peak stress is still less than half the yield strength of Inconel 625 at 1000 °C.

The co-author has demonstrated the manufacturing technique, using a jig and mild steel, plate as part of his capstone project in mechanical engineering. An example of his work is given in figure 4. The material of choice for the final product is Inconel 625. For Inconel, a hot forming process might be required. It is estimated that the production cost will be about two orders of magnitude lower than that of wire cutting.

An alternative design, similar to that of Degroote [10] was also analyzed. The corrugated section is enclosed in a larger tube. The benefit of the alternative configuration is that seam welds along the fins are not required; the end cap is welded directly onto the outer tube. Similarly, the spike is fixed to the outer air plenum by a weld between the outer tube and the dome. At the same time, the outer tube fulfils the function of the retaining rings. On the down side, the surface for heat transfer is reduced substantially, and contact resistance between the outer tubes and fins might further impede heat transfer. Welding the fins to the inside of the tube using induction welding should alleviate the problem.

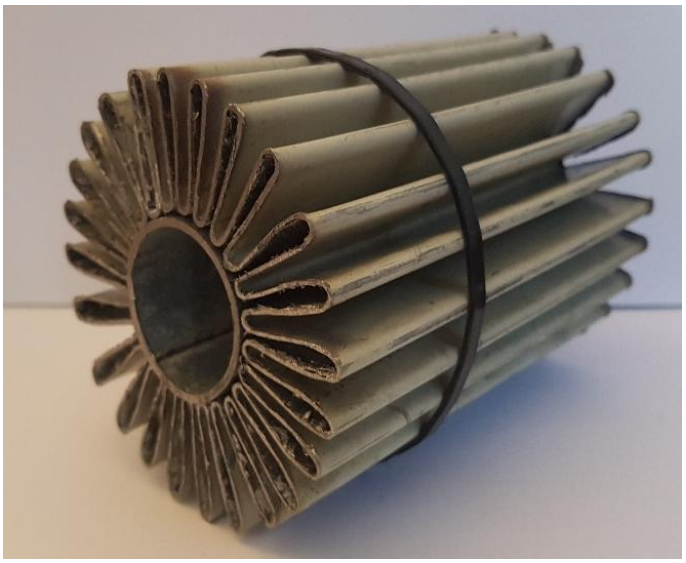

Figure 4. Finished prototype.

The performance of both designs will be compared to Lubkoll's concept, under the same conditions. The receiver comprise of a 4 m diameter sphere mounted on a tower, with spikes protruding in a radial direction. A horizontal plane slices through the receiver, and only the bottom half is irradiated, as shown in figure 1. The centre of the sphere is 82 m above the pivot point of the heliostats. It is assumed that the land is perfectly flat and heliostats are not canted. Following Lubkoll et al's [9] suggestion that small heliostats give the best results, we opted for 1.83 m × 1.22 m heliostats, arranged in a surround

field according to a densely spaced biomimetic arrangement suggested by Noon, Torrilhon and Mitsos [12]. Only cosine, reflection and fouling losses were taken into account. Radiation input at the design conditions were taken from typical meteorological year data for Upington, South Africa. The design point corresponds to solar noon on the autumn equinox in the Southern hemisphere.

3. Simulation setup

Standard, widely available software for solar thermal power plant analyses like NREL's Soltrace [13] and SolarPILOT [14] do not allow for spherical surfaces. Although possible to break the sphere up into flat facets and enter data for each facet, it is rather tedious and does not allow for easy transfer of data between different software products. We opted to do everything in a commercial computational fluid dynamics (CFD) code. Of the radiation models available, only the discrete ordinates model allows for the combination of specular radiation and parallel processing. However, the resource requirement for the large number of beams required for good resolution of solar radiation is excessive. Given our hardware limitations, we adopted a staged approach.

At first, the radiation between the heliostat field and a spherical surface enclosing the receiver is modelled. Radiation intensity from the heliostats towards the receiver is given by

$$I = I_{sol}(A_h/A)\eta_r\eta_f \cos\theta$$

… with I_{sol} the direct normal irradiation from the sun, (A_h/A) the area density of the heliostat field, η_r the clean mirror reflection efficiency, η_f the fouling efficiency and θ the angle between mirror normal and tower vector. The latter is given by

$$\theta = \frac{1}{2}\cos^{-1}(\vec{s}\cdot\vec{t})$$

In the above, $\vec{s}$ is the unit vector pointing towards the sun, whilst $\vec{t}$ is the unit vector pointing from the heliostat to the centre of the receiver. The base of the tower is at the origin of the coordinate system.

For the spherical receiver, our domain comprises of a 30° slice spanning the south-eastern sector to the heliostat field. Domain size is determined by hardware resources, whilst the choice of the south-western sector was arbitrary. The domain is bordered by two vertical symmetry planes, whilst the top of the domain is transparent to let radiation through unimpeded. The receiver is modelled as an absorbing surface with a surface emissivity of $\varepsilon = 0.95$, typical of Pyromark paint [15]. Heliostats are modelled as a transparent wall. Radiation enters the domain as collimated beams in the same direction as the tower vector. User defined functions are used to prescribe the beam direction and intensity based on the computational cell's coordinates. The ground between the heliostat field and tower is modelled as an opaque wall, as was the tower itself.

The domain comprise of 270 000 polyhedral cells, and cells are refined near the receiver for higher resolution. The discrete ordinates radiation model for a single grey band radiation was selected, with 72 divisions in both azimuthal and polar direction, and an 8 × 8 pixilation at cell boundaries. This was the maximum resolution we could achieve on a machine with 16 Xenon E5-2643 processors and 256 GB RAM. Compared to 60 × 60 division, the change in total irradiation on the receiver was less than 5 %, deemed sufficiently small to declare the solution beam independent. Only the radiative transfer equation was solved, using a second order discretization scheme.

A profile of the incident radiation at the surface of the spherical enclosure containing the receiver was saved at the end of the simulation. This profile serves as a radiation input boundary condition for the next stage. Only the magnitude of the radiation is available for export. It was assumed that all the radiation was aimed at the centre of the receiver.

The domain for the second stage includes the air space in a spherical volume, 5 m in radius surrounding the receiver. A cluster of 19 neighbouring spikes were simulated. The effect of cross-winds was neglected, but natural convection was taken into account. This allows us to take advantage of the symmetry conditions. Apart from the symmetry boundary, pressure inlet boundary conditions were prescribed on the bottom, sides and top of the domain. The boundary facing the heliostat field was modelled as a transparent wall, and the radiation profile calculated in the previous stage was prescribed on this boundary. We made the simplifying assumption that the radiation is normal on the domain boundary. Convective boundary conditions are prescribed for the spikes, with the heat transfer coefficient and temperature based upon the average flow conditions inside the spike. These, of course, were only calculated during the third phase. Iteration between the two models was required.

We used the Boussinesq approximation for buoyancy, and adopted Menter's [16] shear stress transport k-ω model as turbulence closure, based on its reasonable performance in predicting separating flows. To aid convergence of buoyancy driven flow, the relaxation factors for pressure and momentum equations were changed to 0.7 and 0.3 respectively [17].

A profile of the incident radiation flux on the spike's outer surface was exported at the end of the simulation. The radiation flux was imported as a boundary condition for the third phase simulations.

No validation data is available to test the integrity of the simulations. A second, independent simulation was done where it was assumed that the incoming radiation flux originates from a point at heliostat level at a distance r from the tower, with

$$r = \sqrt{R_i R_o}$$

… where R_i and R_o are the distance from the inner most and outer most heliostat from the tower. The intensity of the beam was taken as the average of the field intensity at the domain boundary. The solar load model was used to calculate the incident flux on the spike surfaces directly. Results were significantly different. When the incoming radiation profile is patched onto the surface of the domain, and under the assumption that it is normal to the (spherical) boundary surface, radiation penetrates deep into the domain. High temperatures are recorded on the dome and fin roots. When radiation is assumed to come from the middle of the heliostat field, it strikes the domain at an oblique angle. Blocking by neighbouring spikes prevents deep penetration, and the highest temperatures are recorded at the spike tips. The latter gave the highest peak temperatures, and was adopted as worst case scenario. Its results were passed on to the third stage simulations.

For the reference case (Lubkoll et al's geometry [9]), and the modified geometry (fins inside outer tube), the staged approach was dropped and the outer surfaces of the spikes and dome were modelled in detail, as shown in figure 5. The domain spans a 6° slice of the heliostat field, with a symmetry plane slicing through the spike cluster – in figure 5, the domain is mirrored in the symmetry plane. Cell count increased to 1.9×10^6 polyhedral cells, and hardware limit was reached for 36×36 discrete ordinate directions. The benefit of this approach is that the assumption on beam direction is removed, but at the cost of a lower resolution for the discrete ordinates model, and omission of natural convection.

Finally, the internal flow through the spike was simulated. Hardware constraints dictated that we could only model a length of 250 mm from the tip of the spike (total length 1 m), as shown in figure 7. Of interest is the relative performance of the three configurations. Incident solar radiation towards the root of the spike is low compared to the tip, and it is expected that that we would capture the correct trends, despite the truncated domain.

Compressed air at 1 MPa, 624 K enters through the inner tube. These numbers were derived from a compressor compressing ambient air at 300 K and 100 kPa to 1 MPa, assuming that the isentropic efficiency of the compressor is 85 %. A constant velocity boundary condition was prescribed at the inlet, as the flow travels about ten diameters before reaching the dome. A constant pressure boundary is prescribed at the outlet. Flow redistribution between channels in the annular space is slow, and often upwards of 10 000 iterations were required for convergence. Second order upwind discretization schemes were used throughout all simulations. All material properties, except density, are temperature, but not pressure dependent.

4. Results and discussion

Penetration of solar radiation deep into the root of the spike is limited in all cases, as neighbouring spikes tend to cast shades onto each other. The incidence angle of the radiation that did strike the sides of the spikes is so small, that the radiation intensity is highly diluted. The highest radiation flux is recorded at the spike tip, as shown in figure 5. The central spike is at an angle of 30° relative to a horizontal plane through the receiver centre. The choice of 30° was arbitrary, and does not necessarily correspond to the highest surface flux. It should not affect the overall results, as only the relative performance of various spike designs was compared.

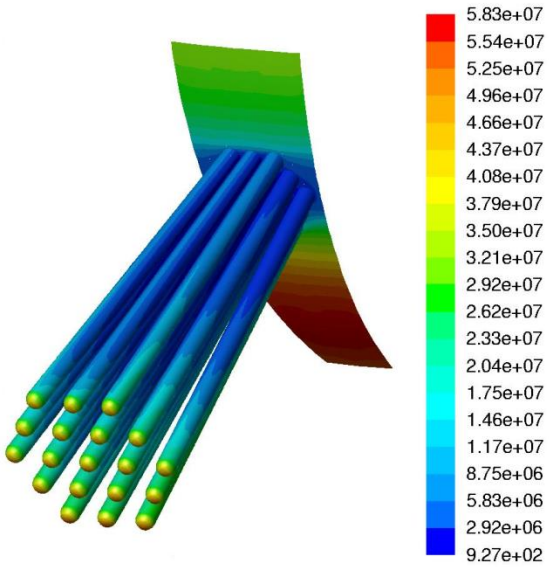

Figure 5. Radiation flux on spike cluster.

The highest metal temperature is recorded at the spike tip, as shown in figure 6 for the reference case. Most of the spike body is effectively at the compressed air inlet temperature of 624 K. This was true for most of the other cases investigated as well.

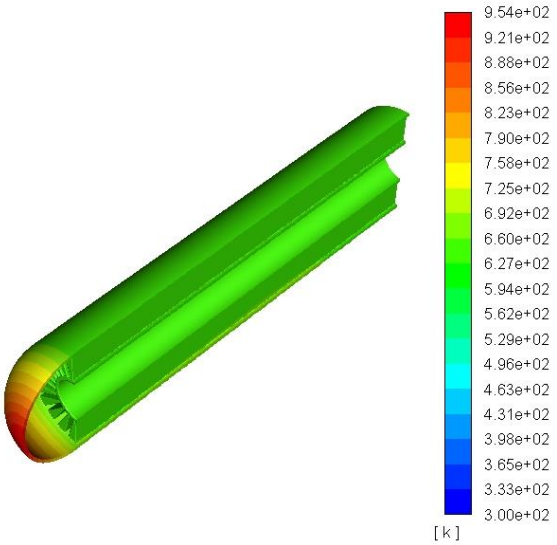

Figure 6. Surface temperatures for reference case.

The increased surface area offered by the corrugated fins (case 1) did not translate into increased absorption of solar radiation, as troughs between the fins are shaded by adjacent fins. With most incoming radiation roughly aligned with the spike axis, the dome large shades the troughs right behind them. The troughs do however trap ambient air between the fins, and convection loss to the environment is somewhat reduced. The flow area for compressed air between the fins is reduced compared to the reference case that results in a large increase in pressure drop. Overall performance of open corrugated fins is worse than that of the reference case.

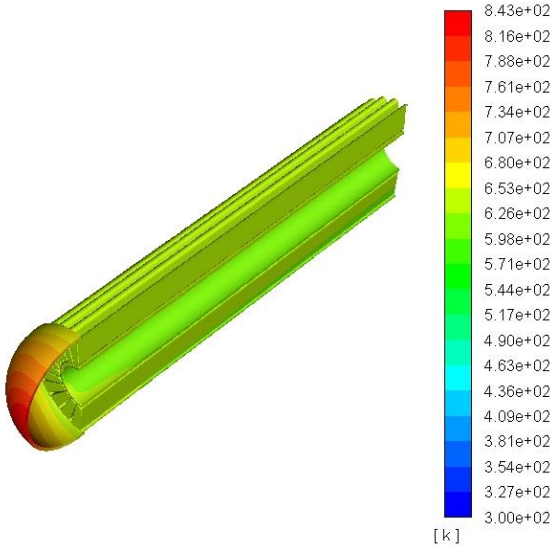

Figure 7

Encasing the corrugated fins inside a sleeve (case 2) increases the flow area available for compressed air, reducing the pressure drop below that of the reference case, whilst heat transfer increases by approximately 3 %. Considering the ease and low cast of manufacture, this would appear to be a feasible solution. No provision was made for contact resistance between the fins and sleeves. In practise, bonding the fins to the sleeve by induction welding may not always lead to a perfect bond.

In case 3, the number of fins was reduced to 18, whilst the fin pitch was increased to 3 mm. This allows for deeper penetration of radiation into the troughs. Although it leads to the largest increase in heat transfer (about 12 %), the pressure drop is still high.

In an attempt to increase the jet impingement velocity onto the inside of the dome, the spike diameter of case 3 was reduced to 65 mm in case 4. Case 4 performs even worse than the reference case.

From the results, it became clear that the highest heat transfer rates are associated with the dome. Enhancing heat transfer in the dome was pursued in case 5. Fins were extended into the dome to near the stagnation point. Although the total heat transfer for case 5 was similar to the reference case, the maximum metal temperature decreased significantly. In retrospect, it became clear that in all sleeved cases (reference, case 2 and case 5), the incident irradiation is approximately the same, hence the total heat transfer is comparable.

Case	**Energy Gain**	**Pressure Drop**
	[Watt]	[Pa]
Reference case	311	700
Case 1 (24 × 20 mm)	191	5 759
Case 2 (Case 1 sleeved)	321	116
Case 3 (18 × 70 mm)	348	2 876
Case 4 (18 × 65 mm)	278	4 928
Case 5 (Ribbed dome)	305	3 822

Table 1. Heat transfer and pressure drop for cases investigated.

5. Conclusion

Corrugated fins offer a distinct manufacturing advantage, both in cost and ease of manufacturing, over the original spiked

concept receiver design. Although thermal stresses in the corrugated spike are higher than in the original design, it is still well below the yield strength of Inconel. A modest increase in heat transfer of about 12 % was achieved for a configuration sporting 18 fins on a fin pitch of 3 mm. However, the gain in heat transfer came at the cost of an increased pressure drop. Optimization of the configuration was not attempted, but will be pursued in the future. Concepts were compared to the original design (reference case), and we strived for designs that fall within the same geometrical constraints as the reference case. Heat transfer enhancement was considered towards the end of the project. Adding ribs on the inside of the dome decreased metal temperatures substantially, reducing the overall radiation loss to the environment. It deserves further investigation. Experimental validation of results is planned for 2018/2019.

Acknowledgements

This study formed part of an undergraduate capstone project in Mechanical Engineering. It was funded by the Department of Mechanical and Mechatronic Engineering at Stellenbosch University.

References

[1] S. Kraemer, (2017), Solar Thermal Power Prices have Dropped an Astonishing 50 % in Six Months, CSP News & Analysis, 29 October 2017, Available from http://www.solarpaces.org/solar-thermal-energy-prices-drop-half

[2] D.G. Kröger, (2012), The Stellenbosch University solar power thermodynamic cycle, http://sterg.sun.ac.za/wp-content/uploads/2012/10/SUNSPOT_July_20121.pdf

[3] A. Kribus et al, (2001), Performance of the Directly-Irradiated Annular Pressurized Receiver (DIAPR) Operating at 20 Bar and 1 200°C, Journal of Solar Energy Engineering Vol. 123(1), pp. 10 – 17.

[4] R. Buck et al, (2002), Solar-hybrid Gas Turbine-based Power Tower Systems (REFOS), Journal of Solar Energy Engineering, Vol. 124 (1), pp. 2 – 9.

[5] I. Hischier, P. Poživil and A. Steinfeld, (2012), A Modular Ceramic Cavity-Receiver for High-Temperature High-Concentration Solar Applications, Journal of Solar Energy Engineering, Vol. 134(1), p. 11004.

[6] L.J. Heller, (2017), Development of a dual-pressure air receiver system for the SUNDISC cycle, PhD Thesis, Stellenbosch University.

[7] A.L. Ávila-Marín, (2011), Volumetric Receivers in Solar Thermal Power Plants with Central Receiver System technology: A review, Solar Energy, Vol. 85, pp. 891 – 910.

[8] C.K. Ho and B.D. Iverson (2014), Review of High-Temperature Central Receiver Designs for Concentrating Solar Power, Renewable and Sustainable Energy Reviews, Vol. 29, pp. 835 – 846.

[9] M. Lubkoll, (2017), Performance Characteristics of the Spiky Central Receiver Air Pre-heater (SCRAP), PhD Thesis, Stellenbosch University.

[10] R.S. Degroote, (1974), Method of Metallurgically a Bonding an Internally Finned Heat Exchange Structure, United States Patent 3 831 247.

[11] R.D McDonald, R.K. Rose and J.W. Papsdorf, (1979), Internally Finned Tube, United States Patent 4 163 474.

[12] C.J. Noone, M. Torrilhon and A. Mitsos, (2012), Heliostat field optimization: A new computationally efficient model and biomimetic layout, Solar Energy, Vol. 86, pp. 792 – 803.

[13] T. Wendelin, A. Lewandowski, A. Dobos, (2012), Soltrace version 2012.9.7, National Renewable Energy Laboratory.

[14] M.J. Wagner, (2016), SolarPILOT version 2016.3.17, National Renewable Energy Laboratory.

[15] C.K. Ho et al, (2013), Characterization of Pyromark 2500 Paint for High-Temperature Solar Receivers, Journal of Solar Energy Engineering, Vol. 136(1), paper 014502, pp. 1 – 4.

[16] F. R. Menter, (1994), Two-Equation Eddy-Viscosity Turbulence Models for Engineering Applications, AIAA Journal, Vol 32(8), pp. 1598 – 1605.

[17] Anonymous, (2017), ANSYS Fluent Tutorial Guide, Available from http://support.ansys.com/training